Biophysical Journal, Volume 97

Supporting Material

Evidence for a Partially Structured State of the Amylin Monomer

Sara M. Vaiana, Robert B. Best, Wai-Ming Yau, William A. Eaton, and James Hofrichter

SUPPLEMETARY INFORMATION

METHODS

Experimental

Sample Preparation: Highly purified, lyophilized hIAPP, rIAPP and cc-AGQ_9 peptides, with amidated C terminus and disulfide bond between Cys2 and Cys7, were supplied by R. Tycko's group, prepared as described by *Luca et al*.(1). Briefly, peptides were synthesized by solid-phase peptide synthesis on an Applied Biosystems 433A synthesizer, cleaved by standard TFA cleavage and purified by HPLC on a C4 reverse phase column (Grace Vydac, Hesperia, CA). Disulfide bond between Cys2 and Cys7 was formed by dissolving the peptide at 1.3 mM in 30% dimethyl sulfoxide (DMSO), 3% acetic acid and letting it react overnight. After disulfide formation the peptide was repurified using a C18 column. Peptide content was analyzed after HPLC purification by electrospray mass spectrometry, giving a molecular weight of 3925Da for W37-hIAPP, 3942 Da for W37-rIAPP and 3230 Da for cc-AGQ_9 (corresponding to the amidated and oxidized form of the peptides). Oxidized peptides were collected, frozen in liquid nitrogen, lyophilized and kept at -20°C.

For each experiment, solutions of monomeric IAPP (rat or human) and cc-AGQ_9 were freshly prepared at T<4°C in deoxy environment similarly to Vaiana et al (2). Buffer was 50mM NaOAc at pH=4.9 with or without 6MGdmHCl. After addition to buffer, the concentration of GdmCl was carefully adjusted to 6M based on refractive index measurements, and the pH to 4.9. The lyophilized peptide was dissolved directly into N_2O saturated buffer solutions. Solutions were then rapidly filtered at 4°C through 0.2μm Anotop10 syringe filters either directly into final cuvettes (for non-aggregating samples) or into glass vials for further separation of monomers from aggregates (for hIAPP in aqueous buffer). hIAPP samples were transferred from glass vyals to centrifuge cells, preequilibrated at 4°C, and centrifuged at 60krpm (=485,000g) for 2hours using a Beckman Coulter Optima XL-100K preparative ultracentrifuge with SW60Ti rotor at T=4°C. The supernatant (<2/3 of total solution volume) was carefully transferred in deoxy environment to a sealed, N_2O saturated 1cm quartz cuvette for measurements. The final peptide concentration in solution was around 60μM. Analytical ultracentrifugation performed on samples used for experiments (both rIAPP and hIAPP) showed that the peptide was all monomeric (as in Ref. (2)). The absence of fibril formation during measurements was confirmed by the reversibility of rates measured at 5°C at the beginning at end of each temperature scan. Electrospray mass

spectrometry performed at the beginning and end of experiments gave molecular weights corresponding to the amidated and oxidized form of the monomeric peptides, confirming that the disulfide bond remained intact during measurements. For viscosity dependent measurements, sucrose was added either to buffer solutions prior to addition of peptide or to final samples. Viscosity of sucrose solutions was measured using a Wells-Brookfield Model LVT cone-plate viscometer with a thermostatted sample chamber.

Tryptophan Triplet Quenching Experiments: The dynamics of end-to-end contact formation were measured by monitoring the lifetime of the triplet state of tryptophan (at the C-terminus of the peptide), which is quenched by close contact with cystine and disulfides (at the N-terminus of the peptide) (3, 4). The tryptophan is excited to its triplet state by a nanosecond UV laser pulse and the population of the triplet state as a function of time is monitored by time-resolved triplet-triplet absorption. For each sample, measurements were performed as a function of temperature at values ranging from 0º to 50ºC. A set of 5 time traces, resulting from an average of 256 laser pulses each, was collected at each condition. Viscosity-dependence of the quenching rates was measured in sucrose solutions at concentrations ranging from 0 to 40% w/w in Buffer and 0 to 32% w/w in GdmCl.

Analysis of Tryptophan Triplet Quenching Data: The raw kinetic data were first analyzed as described by Lapidus et al. to produce a set of signal amplitudes (proportional to tryptophan triplet population), evenly spaced on a log(t) grid. Data noise reduction was obtained by either averaging over the 5 traces collected for each condition, or by using the singular value decomposition (SVD) method described in the following. Both methods generated essentially the same rates, with SVD having a reduced noise level (SVD results shown throughout the paper). The temperature- and viscosity-dependent kinetic data for each set of buffer conditions were assembled into an array containing approximately 30 traces. This array was then decomposed using SVD and the results examined to assure consistency of amplitudes with experimental conditions. The data array was then reconstructed from the twelve largest SVD components for further analysis (examples shown in Figs.2,4, SI2). This array was then used as input in either of the two fitting procedures described below.

Independent Fits to Determine Relaxation Rates k_{obs} at each Temperature (Fig.2-4)

Data were initially independently fit to an exponential relaxation, together with a time-independent offset and a second offset function which was constant for times less than 10^{-4} s and

varied linearly with log(*t*) for times longer than 10^{-4} s (empirically accounting for the observed slower decay due to a radical photoproduct (3)). This yielded the exponential relaxation rates (k_{obs}), which are plotted as a function of temperature for each peptide and solution condition in Fig. 3. For the sake of simplicity we shall first assume in the discussion of our results, that the observed changes in k_{obs} reflect changes in the end-to-end equilibrium distribution, with rates getting faster when the end-to-end distance distribution favors shorter distances. The more accurate analysis described below, which accounts for potential changes in both the end-to-end distance distribution and end-to-end diffusion shows that this is indeed the case.

Global Fits to Determine Reaction- and Diffusion- Limited Rates from Viscosity Dependence (Fig.SI2-SI4)

Quenching of the tryptophan triplet state by end-to-end contact formation with cystine can, to a good approximation, be described by a simple two-step kinetic model (3, 5). In this model, the ends of the peptide first diffuse together with rate k_{D+} to form an encounter complex; the cystine then either quenches the tryptophan triplet state with rate q or diffuses away with a rate $k_{D!}$. The observed quenching rate (k_{obs}) is given by:

$$k_{obs} = k_{D+} \frac{q}{k_{D-} + q} \equiv k_{D+} \phi \qquad (1)$$

where the quenching yield, ϕ, is the probability of quenching during the lifetime of the encounter complex. Diffusion-limited rates k_{D+} can be obtained by measuring the dependence of the quenching rates on solution viscosity. Equation (1) can be rearranged to give:

$$\frac{1}{k_{obs}} = \frac{1}{k_R} + \frac{1}{k_{D+}} \qquad (2)$$

where the reaction-limited rate, k_R, is that measured when $k_{D-} >> q$. Under these conditions, $k_R = qK_{eq}$, where K_{eq} ($= k_{D+}/k_{D-}$) is the equilibrium constant for forming the encounter complex and the fraction of encounter complexes is equal to its equilibrium value at all times. Since k_R depends only on the distribution of end-to-end distances in the unfolded chain and q it can be used to explore the conformation of unfolded chains. For example, increasing the average end-to-end distance by increasing chain length or by swelling the chain via repulsive interactions will decrease K_{eq} and therefore decrease k_R. The diffusion-limited rate, k_{D+}, is the measured rate when $q >> k_{D-}$, and corresponds to the rate of bringing the ends together to form a short-range contact.

Reaction limited and diffusion-limited rates can be obtained experimentally by measuring the dependence of the observed quenching rates on solution viscosity. By plotting $1/k_{obs}$ versus solution viscosity, $1/k_R$ is obtained from the intercept at zero viscosity and the diffusion limited time for contact formation, $1/\eta k_{D+}$, is obtained from the slope. To fit the data, we assume that the rates k_R, and k_{D+} can be empirically described at each temperature by:

$$k_R = k_R(T)$$
$$k_{D+} = f(\eta)k_{D+}(T) = \left[\eta(1-A\eta)\right]^{-1} k_{D+}(T) \quad (3)$$

where T is the temperature, η the solution viscosity measured at the given temperature and A is a fitting parameter which is used to describe the nonlinear viscosity-dependence observed at low temperatures and high sucrose concentrations. This curvature needs be accounted for in order to obtain accurate values for the intercepts and initial slopes of the experimental data.

Temperature- and viscosity-dependent experimental data, for each peptide under each set of solution conditions, was globally fitted with a set of exponential relaxations, together with a time-independent offset and a second offset function which was constant for times less than 10^{-4} s and varied linearly with log(t) for times longer than 10^{-4} s. The output is an array of values for $k_R(T)$ and $k_{D+}(T)$ (equation 3) for each temperature together with the value of A. A sample of the resulting fits for cc-AGQ_9 in 6 M GdmCl is shown in Figure SI3.

Reduction of the N-terminal Disulfide (Fig.SI8)

A control experiment on the reduced form of cc-$(AGQ)_9$ was performed after adding TCEP to final solutions. Results comparing the oxy and reduced forms of the peptide in 6MGdmCl and Buffer at 10°C are shown in Figure SI8. For consistency of comparison, data for the reduced peptide were independently fit as described above for the oxy peptide. This yielded the exponential relaxation rates (k_{obs}) shown in the Table of Figure SI8 for 20°C (values for 10C shown in parenthesis). Similarly to c-$(AGQ)_9$, the quenching rate for the reduced peptide increases only by a factor 2 in going from Buffer to 6M GdmCl, at variance with the factor 9 found for the oxy peptide. This rules out the possibility that collapse is due to the addition of the particular C-terminal sequence, rather than to the disulfide loop. If collapse was due to the sequence, irrespective of the formation of the loop, we would observe the same degree of chain compaction in buffer for the reduced and the oxy form of the peptide.

We note that the faster absolute quenching rate (~5x) for reduced cc-$(AGQ)_9$ compared with the oxidized form in denaturant can be explained by the presence of two cys quenchers, instead of just one cystine. The combination of this effect with the much smaller collapse of the reduced peptide results in the absolute quenching rates being similar in buffer. A quantitative understanding of the effect of two quenchers would require further studies, however this would not affect our conclusions.

Molecular Dynamics Simulations:

Molecular dynamics simulations of c-$(AGQ)_9$ and cc-$(AGQ)_9$ were run in explicit solvent using the GROMACS (6) molecular simulation package. The peptide and ions were described using the GROMACS port (7) of the Amber03 protein force field, and water using the TIP3P water model (8). A random coil initial conformation of each peptide was solvated by placing it in a 50 Å cubic box of water and deleting water molecules within 2.8 Å of the solute. The system was neutralized by adding 6 sodium and 7 chloride ions inserted by replacement of randomly chosen water molecules. Initial configurations were chosen at 50 ps intervals from a constant volume simulation at 800 K. For each peptide, eight long simulations of 94 ns each were run, each starting from a different initial configuration, for a total of ~ 0.75 μs of data. The temperature was maintained at 300 K using a Nose-Hoover (9, 10) thermostat and pressure at 1 atm with a Parinello-Rahman (11) barostat. All bonds to hydrogen were constrained with the SHAKE (12) algorithm and a time step of 2 fs was used. Electrostatic interactions were treated using particle mesh Ewald (13, 14) with a grid spacing of 1.2 Å.

Simulations of hIAPP and rIAPP were also run using the procedure described above. In addition, a separate set of simulations of the amylin peptides was run in which the initial states

$$E_Q = \frac{1}{2} k_Q (Q - Q_0)^2$$

were generated at a high temperature (800K), but with a bias potential to favour the formation of contacts found in the average contact map with a frequency of greater than 0.3 in the cc-AGQ_9 simulations. The following potential was used:

$$Q = \frac{1}{N_{ij}} \sum_{(i,j)} \frac{1}{1 + \exp(\gamma(r_{ij} - r_0))}$$

where Q_0=1 and the fraction of Cα-Cα contacts Q was defined as:

Here, the reference distance r_0 was taken as 8.0 Å for each contact and $\gamma = 5.0$. Several 20 ns trajectories at 300 K were then carried out starting from configurations chosen at random from this ensemble.

1. Luca, S., W. M. Yau, R. Leapman, and R. Tycko. 2007. Peptide conformation and supramolecular organization in amylin fibrils: Constraints from solid-state NMR. Biochemistry 46:13505-13522.

2. Vaiana, S. M., R. Ghirlando, W. M. Yau, W. A. Eaton, and J. Hofrichter. 2008. Sedimentation studies on human amylin fail to detect low-molecular-weight oligomers. Biophysical Journal 94:L45-L47.

3. Lapidus, L. J., W. A. Eaton, and J. Hofrichter. 2000. Measuring the rate of intramolecular contact formation in polypeptides. Proceedings of the National Academy of Sciences USA 97:7220-7225.

4. Lapidus, L. J., P. J. Steinbach, W. A. Eaton, A. Szabo, and J. Hofrichter. 2002. Effects of chain stiffness on the dynamics of loop formation in polypeptides. Appendix: Testing a 1-dimensional diffusion model for peptide dynamics. Journal of Physical Chemistry B 106:11628-11640.

5. Lapidus, L. J., W. A. Eaton, and J. Hofrichter. 2002. Measuring dynamic flexibility of the coil state of a helix-forming peptide. Journal of Molecular Biology 319:19-25.

6. Lindahl, E., B. Hess, and D. van der Spoel. 2001. GROMACS 3.0: a package for molecular simulation and trajectory analysis J. Mol. Model. 7:306-317.

7. Sorin, E. J., and V. S. Pande. 2005. Exploring the helix-coil transition via all-atom equilibrium ensemble simulations Biophys. J. 88:2472-2493.

8. Jorgensen, W. L., J. Chandrasekhar, and J. D. Madura. 1983. Comparison of simple potential functions for simulating liquid water. J. Chem. Phys. 79:926-935.

9. Hoover, W. G. 1985. Canonical dynamics: equilibrium phase-space distributions. Phys. Rev. A 31:1695-1697.

10. Nosé, S. 1984. A molecular dynamics method for simulations in the canonical ensemble. Mol. Phys. 52:255-268.

11. Parinello, M., and A. Rahman. 1981. Polymorphic transitions in single crystals: a new molecular dynamics method. J. Appl. Phys. 52:7182-7190.

12. Ryckaert, J. P., G. Cicotti, and H. J. C. Berendsen. 1977. Numerical integration of the cartesian equations of motion of a system with constraints: molecular dynamics of n-alkanes. J. Comp. Phys. 23:327-341.

13. Darden, T., D. York, and L. Pedersen. 1993. An N-log(N) method for Ewald sums in large systems. J. Chem. Phys 103:8577-8592.

14. Essmann, U., L. Perera, M. L. Berkowitz, T. Darden, H. Lee, and L. G. Pedersen. 1995. A smooth particle mesh ewald potential. J. Chem. Phys 103:8577-8592.

Figure SI-1

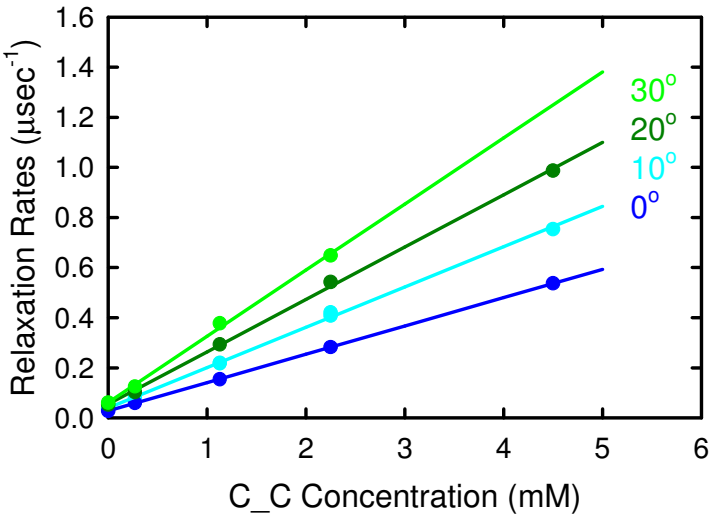
Relaxation Rates (µsec-1)
C_C Concentration (mM)
30°
20°
10°
0°
0.0
0.2
0.4
0.6
0.8
1.0
1.2
1.4
1.6
0
1
2
3
4
5
6

Figure SI-2

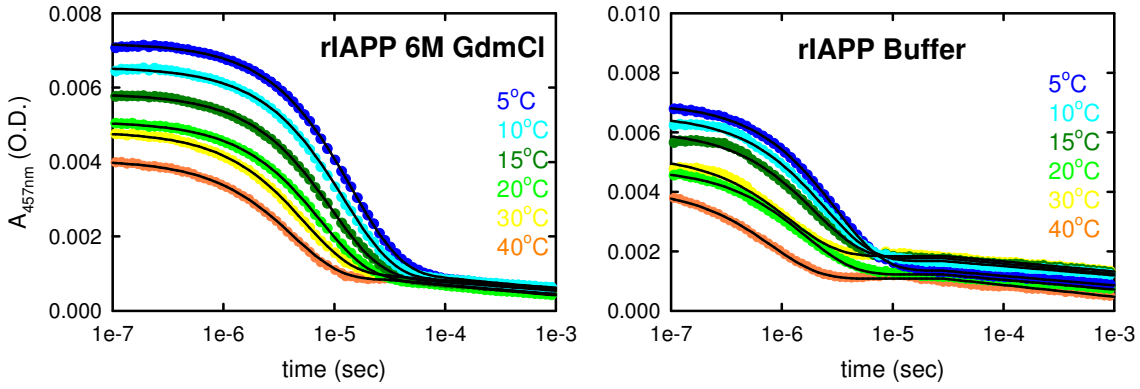
rIAPP 6M GdmCl
5°C
10°C
15°C
20°C
30°C
40°C
A457nm (O.D.)
0.008
0.006
0.004
0.002
0.000
1e-7
1e-6
1e-5
1e-4
1e-3
time (sec)
rIAPP Buffer
0.010
0.008
0.006
0.004
0.002
0.000
time (sec)

Figure SI-3

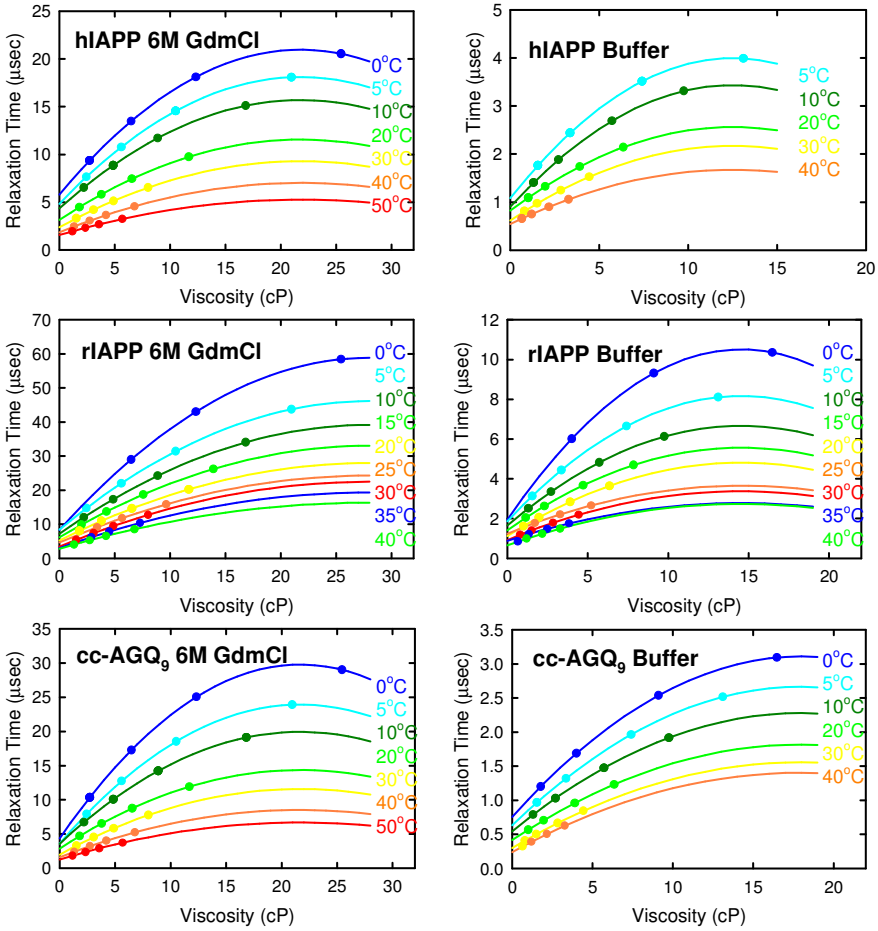
hIAPP 6M GdmCl
0°C
5°C
10°C
20°C
30°C
40°C
50°C
hIAPP Buffer
5°C
10°C
20°C
30°C
40°C
rIAPP 6M GdmCl
0°C
5°C
10°C
15°C
20°C
25°C
30°C
35°C
40°C
rIAPP Buffer
0°C
5°C
10°C
15°C
20°C
25°C
30°C
35°C
40°C
cc-AGQ9 6M GdmCl
0°C
5°C
10°C
20°C
30°C
40°C
50°C
cc-AGQ9 Buffer
0°C
5°C
10°C
20°C
30°C
40°C
Relaxation Time (µsec)
Viscosity (cP)

Figure SI-4

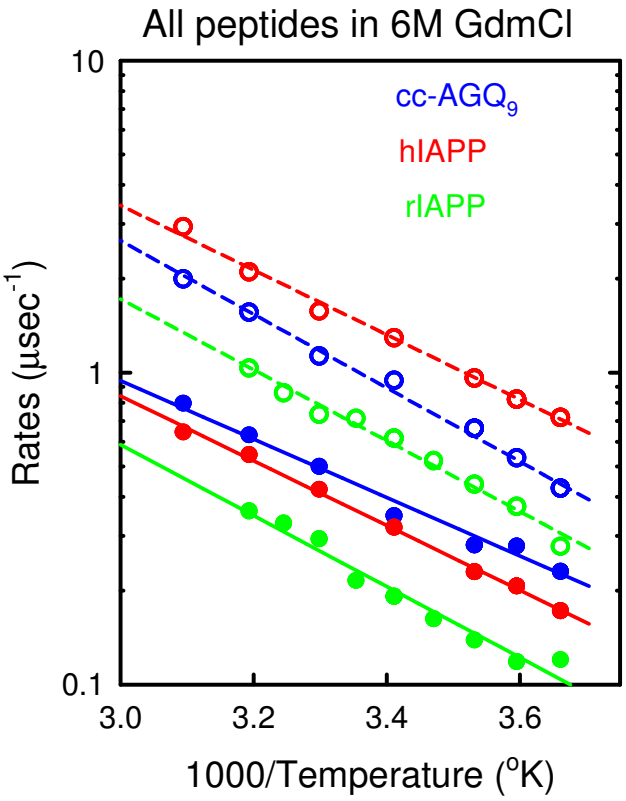
All peptides in 6M GdmCl
cc-AGQ9
hIAPP
rIAPP
Rates (μsec-1)
10
1
0.1
3.0
3.2
3.4
3.6
1000/Temperature (°K)

Figure SI-5

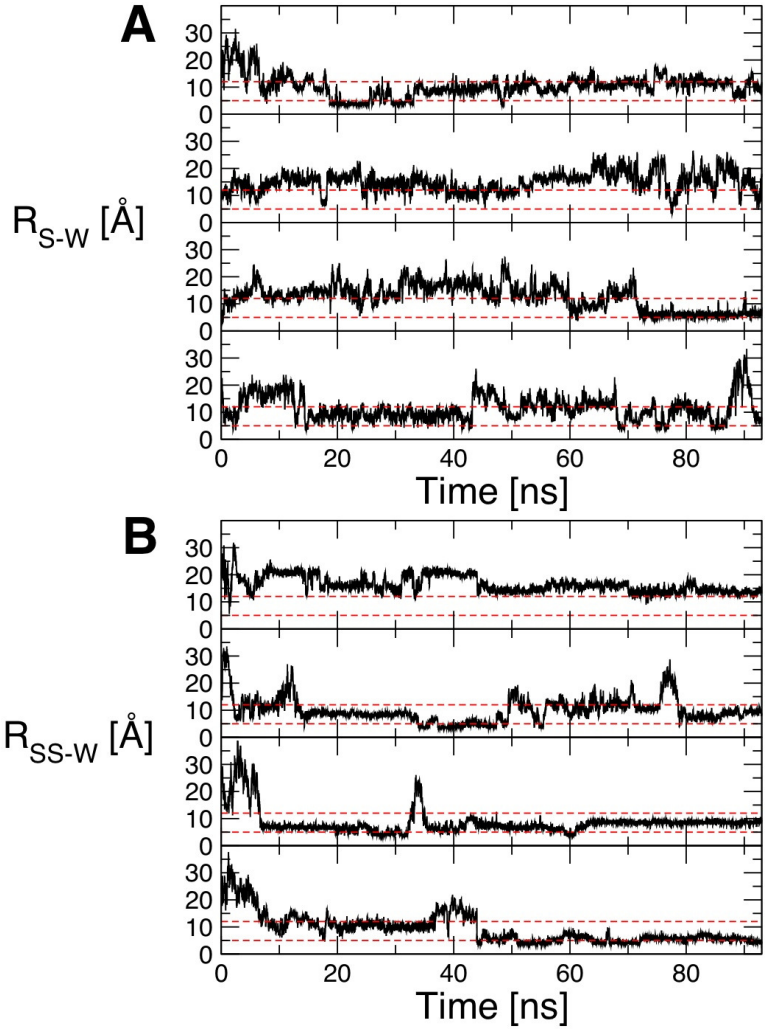

Figure SI-6

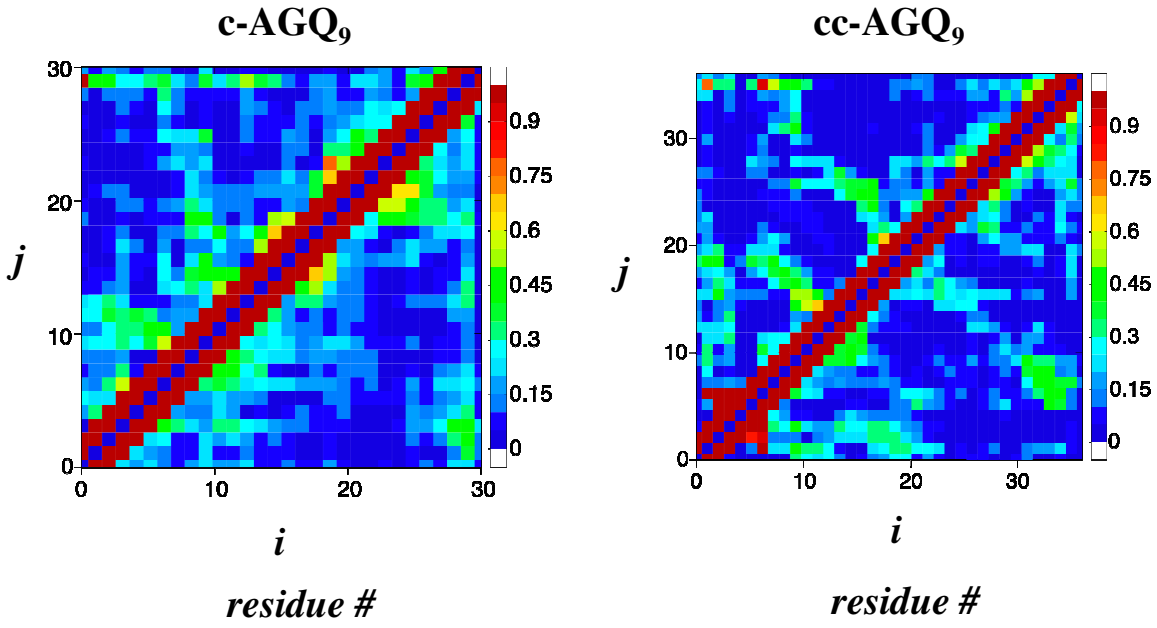

Figure SI-6. Contact maps calculated from the 'contact' (upper left quadrant) and 'kinked' (lower right quadrant) subsets of trajectories for c-$(AGQ)_9$ (A) and cc-$(AGQ)_9$ (B).

Figure SI-7

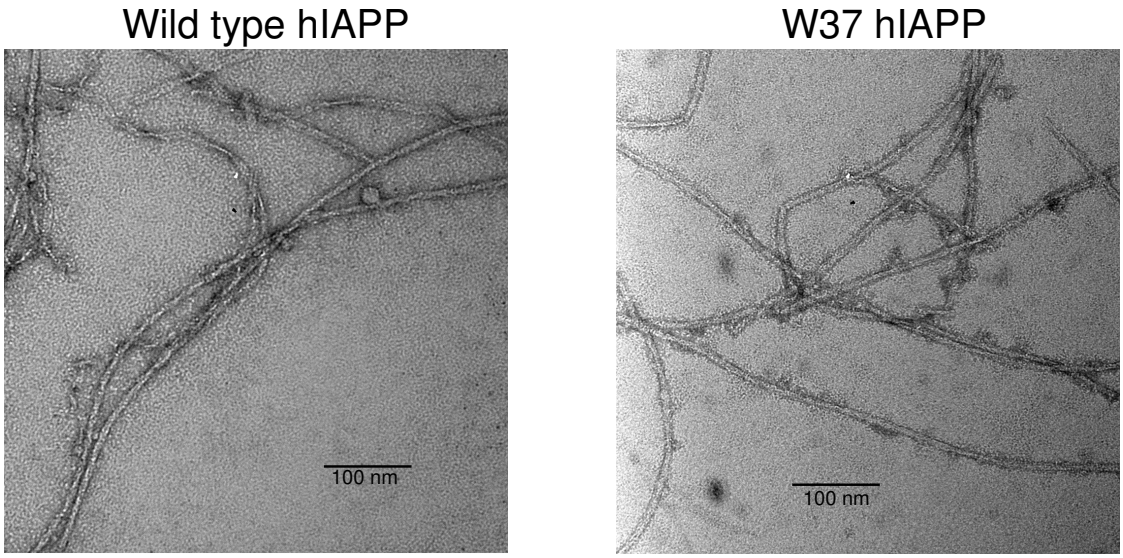

Figure SI-8

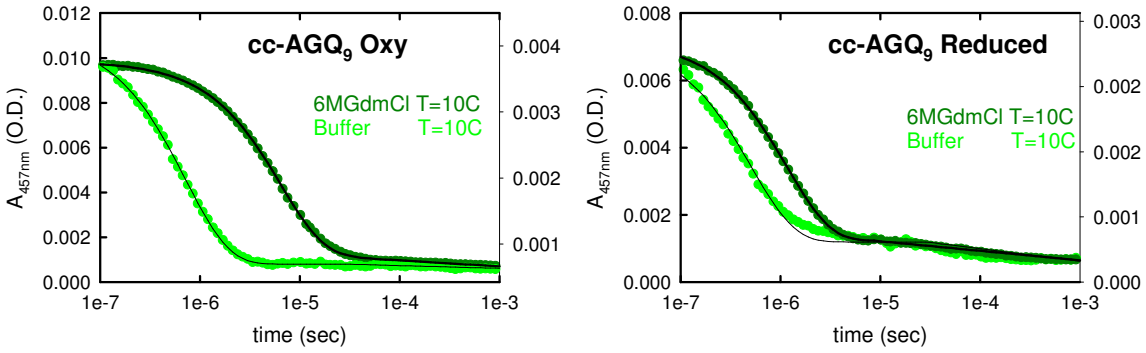

Peptide	k_{obs} (μsec^{-1})	
	Buffer	*6M GdmCl*
Oxy	2.0 (1.4)	0.21 (0.15)
Reduced	2.0 (1.9)	1.1 (0.82)